ChemPubSoc Europe

DOI: 10.1002/cctc.201700127

CHEMCATCHEM Full Papers

Silica-Supported Au–Ag Catalysts for the Selective Hydrogenation of Butadiene

Nazila Masoud,[a] Laurent Delannoy,[b] Christophe Calers,[b] Jean-Jacques Gallet,[c] Fabrice Bournel,[c] Krijn P. de Jong,[a] Catherine Louis,[b] and Petra E. de Jongh*[a]

Gold and silver are miscible over the entire composition range, and form an attractive combination for fundamental studies on bimetallic catalysts. Au–Ag catalysts have shown synergistic effects for different oxidation and liquid-phase hydrogenation reactions, but have rarely been studied for gas-phase hydrogenation. In this study 3 nm particles of Au, Ag and Au–Ag supported on silica (SBA-15) were investigated as catalysts for selective hydrogenation of butadiene in an excess of propene. The Au catalyst was over an order of magnitude more active than the Ag catalyst at 120 °C. The initial activity of the Au–Ag catalysts scaled linearly with the Au-content, suggesting a direct correlation between the surface and overall compositions of the nanoparticles and the absence of synergistic effects. All Au-containing catalysts were highly selective to butenes (>99.9%). The Au catalysts were stable, whereas the Au–Ag catalysts lost about half of their activity during 20 h run time at 200 °C, but the initial activity was restored by a consecutive oxidation-reduction treatment. Near ambient pressure x-ray photoelectron spectroscopy showed that exposure to H_2 at elevated temperatures led to a gradual enrichment of the surface of the Au–Ag nanoparticles by Ag. These observations highlight the importance of considering progressive atomic rearrangements in bimetallic nanocatalysts under reaction conditions.

Introduction

Supported Au catalysts have been studied for a wide range of oxidation and hydrogenation reactions since the mid-80's when Haruta discovered the high activity of Au nanoparticles in CO oxidation.[1] Gold selectively catalyzes the hydrogenation of unsaturated aldehydes,[2] esters,[3] acetylene in the presence of an excess of ethylene,[4] as well as butadiene in the presence of an excess of alkenes.[5] A potential application is the removal of polyunsaturated (alkynes and alkadienes) impurities from alkene feedstocks for polyolefin production. Alkenes streams that are produced from the cracking of naphtha and gas oil contain polyunsaturated impurities, such as acetylene, propyne, or butadiene. These impurities can poison polymerization catalysts, and thus must be selectively hydrogenated to alkenes with residual concentrations lower than 10 ppm without over-hydrogenation to alkanes.[5,6] In industry, palladium-based catalysts are used to reduce the butadiene concentration from 1% to 100 ppm or less in a C4 alkene gas stream through selective hydrogenation.[7] The development of a more selective catalyst, that reaches full conversion of butadiene without conversion of any alkenes, is desirable.

Gold catalysts are very selective for this reaction, but far less active than Pd catalysts.[5] For example, in the hydrogenation of acetylene at 30 °C, the activity of Au is about two orders of magnitude lower than that of Pd.[5] To increase the activity of the catalyst for hydrogenation reactions, Au has been alloyed with other metals, such as Pd,[8] Pt,[9] and Ni,[10] but this led to lower selectivities than for Au alone. For instance, for the hydrogenation of butadiene with an excess of propene, it is reported that at the lowest temperature that yields full conversion of butadiene, the propene conversion to propane is 0.03% if catalyzed by Au, whereas it is 0.3% if it is catalyzed by Au-Pd with Au to Pd atomic ratio of 20.[11]

Cu as well as Au-Cu nanoparticles have shown catalytic activity and selectivity for the hydrogenation of butadiene.[12] Silver catalysts selectively catalyze different hydrogenation reactions[13] such as the hydrogenation of unsaturated aldehydes, for instance, acrolein, crotonaldehyde,[14] or citral,[15] and hydrogenation of unsaturated esters,[16] nitroaromatics,[17] and acetylenic compounds.[18] Grünert et al. reported that for the hydrogenation of unsaturated aldehydes, the only monometallic

[a] N. Masoud, Prof. Dr. K. P. de Jong, Prof. Dr. P. E. de Jongh
Inorganic Chemistry and Catalysis
Debye Institute for Nanomaterials Science
Utrecht University
Universiteitweg 99, 3584 CG Utrecht (The Netherlands)
E-mail: P.E.deJongh@uu.nl

[b] Dr. L. Delannoy, C. Calers, Dr. C. Louis
Laboratoire de Réactivité de Surface
Sorbonne Universités, UPMC Univ Paris 06, UMR CNRS 7197
4 Place Jussieu, Case 178, F-75252, Paris (France)

[c] Dr. J.-J. Gallet, Dr. F. Bournel
Laboratoire de Chimie Physique-Matière et Rayonnement
Sorbonne Universités, UPMC Univ Paris 06, CNRS
11 rue Pierre et Marie Curie, 75005 Paris (France)
and, Synchrotron-Soleil
L'orme des Merisiers, Saint Aubin—BP48 91192,
Gif-sur-Yvette Cedex (France)

Supporting information and the ORCID identification number(s) for the author(s) of this article can be found under https://doi.org/10.1002/cctc.201700428.

This manuscript is part of a Special Issue on the "French Conference on Catalysis".

metals selective to allyl alcohol products are Ag and Au.[19] According to a computational study by Nørskov et al., Ag is more active than Au in H_2 dissociation,[20] and Cu is more active than Ag. Copper catalysts are indeed more active than Au catalysts in alkyne hydrogenation.[12,21]

Au–Ag catalysts have been extensively studied for oxidation reactions,[22] but have been less explored for hydrogenation reactions. The main studies on hydrogenation focus on liquid-phase rather than gas-phase catalysis. For instance Au–Ag catalysts showed much higher activity than monometallic Au and Ag catalysts for the selective hydrogenation of dimethyl oxalate to methyl glycolate and ethylene glycol in the liquid-phase.[16] The Au–Ag catalysts also showed activity for the selective hydrogenation of acetylene in the presence of excess ethylene.[23] To the best of our knowledge, the catalytic properties of Au–Ag catalyst for the selective hydrogenation of butadiene have not been studied yet.

Apart from activity and selectivity, catalyst stability is a crucial factor for industrial applications.[24] For bimetallic catalysts, many examples in the literature show higher stability than their monometallic equivalents.[25] Zanella et al. demonstrated that titania supported Au–Ag[22a] and Au–Cu catalysts[26] show a higher stability than Au catalysts in CO oxidation reactions.

Common deactivation mechanisms are particle growth, coke deposition, and catalyst leaching or poisoning.[7b] For bimetallic catalysts, redistribution of atoms within the nanoparticles owing to reaction conditions (elevated temperature, oxidative or reductive atmosphere) can in addition play an important role. For example, Fe segregates to the surface of Fe–Pt, Fe–Rh, and Fe–Au under O_2 atmosphere at 250 °C,[27] and Cu moves to the surface of Co–Cu if it is exposed to H_2 and to the core if it is exposed to CO at 370 °C.[28]

Au–Ag nanoparticles are a very interesting model system owing to similarity of Au and Ag in lattice spacing and hence miscibility of these two metals over the entire composition range. Ag has a lower surface tension and has a higher affinity for oxygen than Au, hence in Au–Ag systems, Ag atoms tend to segregate to the surface under oxidative conditions.[22a,23a] However, the surface composition of bimetallic Au–Ag nanoparticles under H_2 atmosphere has not been reported yet.

In this paper, we discuss the selectivity, activity, and the stability of the Au–Ag as well as Au and Ag catalysts for the selective hydrogenation of butadiene in a gas stream containing an excess of propene. As a support we chose an ordered mesoporous silica (SBA-15)[29] with uniform hexagonally arranged pores and a narrow pore size distribution. It has a high specific surface area, facilitating the preparation of small particles and an even distribution of metal particles over the support. Surface functionalization of the silica support with aminopropyl groups facilitates the preparation of small Au and Au–Ag nanoparticles and a homogenous distribution over the support. The activities of Au, Ag and Au–Ag catalysts with different compositions but with similar, all 3 nm, particle sizes in gas-phase hydrogenation are compared. An interesting question is how active Ag is for this type of reaction, and whether synergistic effects, resulting from either electronic or ensemble effects, on the activity are observed in the case of the bimetallic catalysts. We are also interested particularly in the stability of the different catalysts. Furthermore near-ambient pressure x-ray photoelectron spectroscopy is used as an important tool to detect changes in the atomic distribution of Au and Ag over the nanoparticles. We will show that there is a correlation between surface composition and the activity and stability for these bimetallic Au–Ag catalysts.

Results and Discussion

Structural characterization

Structural properties of the catalysts are summarized in Table 1. Transmission electron microscopy (TEM) images (Figure 1 a–d) show that particles with an average size of 2–4 nm are present inside the 8 nm pores of the ordered mesoporous silica. Inductively coupled plasma-mass spectrometry (ICP-MS) confirmed the intended Au and Ag loadings. Nitrogen physisorption isotherms (Figure S.1) showed a loss of support porosity upon Au deposition, but no significant change in the pore size of the silica. Thermogravimetric analysis (TGA)

Table 1. Structural properties of the silica supported Au, Ag, and Au–Ag catalysts.

Catalyst	Particle size [nm][a]	Au loading [wt%]	Ag loading [wt%]	Atomic Au:Ag ratio
Au	2.6±0.5	3.7	0	1:0
Au3Ag1	2.9±0.6	2.6	0.5	3:1
Au2Ag1	3.1±0.8	2.1	0.7	1.7:1
Ag	2.9±0.8	0	1.8	0:1

[a] Number-averaged diameter calculated as $\Sigma n_i d_i / \Sigma n_i$, in which d_i is the individual particle diameter.

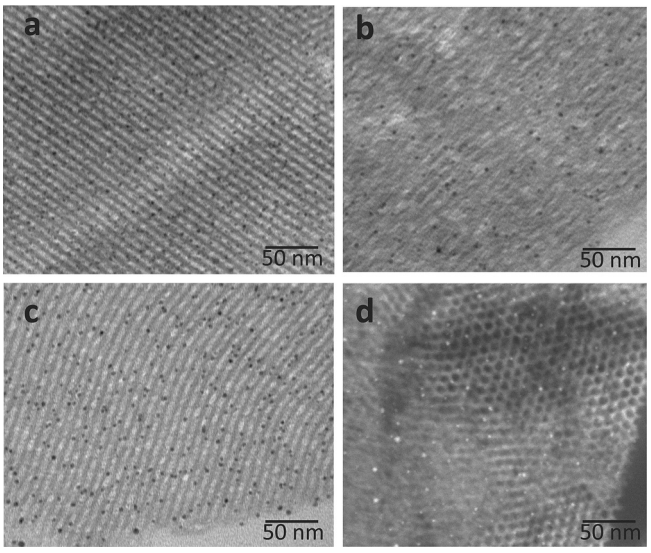

Figure 1. Bright field TEM images of the Au (a), Au3Ag1 (b), and Au2Ag1 (c) catalysts, and high angle annular dark-field-scanning TEM images of the Ag catalyst (d).

(Figure S.2) showed that the removal of aminopropyl groups started at 250 °C, and that all aminopropyl had been removed after calcination for 4 hours at 450 °C. Hence, these 3 nm Au, Ag and Au–Ag particles on SiO_2 with 3 wt.% metal loading and well-defined composition range form the basis for the studies presented in this paper.

Ultraviolet-visible (UV/Vis) absorption spectra (Figure 2) show clear surface plasmon resonance absorption for all samples after calcination. For the Ag nanoparticles the maximum absorption occurs at 390 nm, whereas it occurs at 510 nm for the supported Au nanoparticles. The maximum absorption for the Au–Ag catalyst lies in between these two values; at 500 nm and 485 nm for the Au3Ag1 and Au2Ag1 catalysts, respectively. No remaining peaks at the Au or Ag absorption wavelength are observed for the bimetallic samples suggesting alloy formation for the Au–Ag nanoparticles.[30]

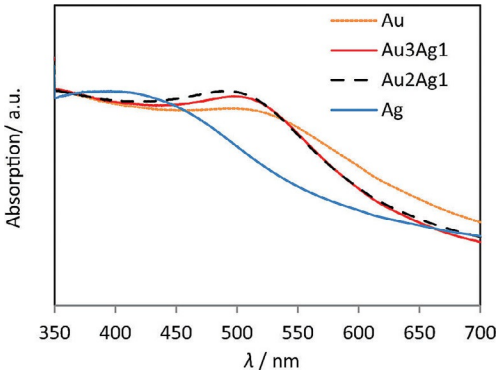

Figure 2. Ultraviolet-visible absorption spectra of the Au, Au3Ag1, Au2Ag1, and Ag catalysts.

Activity

The butadiene conversions in the temperature range of 50–300 °C for the in situ reduced Au, Ag and bimetallic Au–Ag catalysts are shown in Figure 3. An overview of the activities at 120 °C and apparent activation energies for these catalysts is given in Table 2. The Au catalyst starts to hydrogenate butadiene at 60 °C and fully converts the butadiene at 225 °C and above. The in situ reduced Au catalyst is slightly more active than the not reduced catalyst (Figure S.3 a): the in situ reduction increases the activity of the catalyst at 120 °C from 6.5 to 8.7 $\mu mol\,s^{-1}\,g_{Au}{}^{-1}$. The apparent activation energy for in situ reduced Au catalyst for butadiene hydrogenation is 49.4 ± 0.7 $kJ\,mol^{-1}$, as obtained from the Arrhenius plot shown in Figure S.4. This value is similar to the reported value of 50 ± 2 $kJ\,mol^{-1}$ for Au/TiO_2 prepared by deposition-precipitation with urea[31] suggesting that the apparent activation energy does not strongly depend on the support, in agreement with the literature.[5] The turnover frequency (TOF) at 150 °C ($9.9\times10^{-3}\ s^{-1}$) is also in good agreement with the value reported by Haruta et al. for the hydrogenation of butadiene at 150 °C ($6\times10^{-3}\ s^{-1}$, Au on silica catalyst prepared by gas-phase grafting, 7.0 ± 3.0 nm).[32] Hence, the activity of our Au catalyst, if reduced in situ, is in good agreement with literature.[31] All results discussed from now on are on in situ reduced catalysts unless stated otherwise.

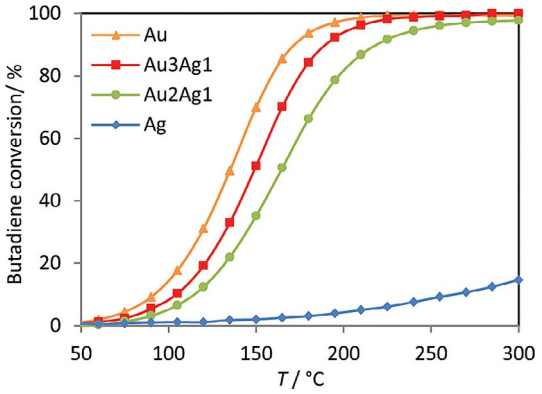

Figure 3. Butadiene conversions for the in situ reduced Au, Ag, Au3Ag1, and Au2Ag1 catalysts for the hydrogenation of butadiene while heating from 50 to 300 °C with 1 °C min^{-1}. Reaction mixture: 0.3% butadiene, 30% propene, 20% H_2, and He for balance at atmospheric pressure, flow rate 50 mL min^{-1}, GHSV 11 700 h^{-1}.

Table 2. Activities and Turnover Frequencies (TOF) of the Au, Ag, and Au–Ag catalysts at 120 °C for the hydrogenation of butadiene.

	Particle sizes[a] [nm]	Activity [$\mu mol\,s^{-1}g_{Au}{}^{-1}$]	TOF[b] [$10^{-13}\ s^{-1}$]	E_{act} [$kJ\,mol^{-1}$]	lnA[c]
Au	3.0	8.7	4.4	49.4 ± 0.7	17.3 ± 0.2
Au3Ag1	3.1	7.7	5.4	52.3 ± 1.2	17.9 ± 0.4
Au2Ag1	3.4	6.1	5.6	55.7 ± 1.5	19.1 ± 0.5
Ag	3.4	0.6[d]	0.2[d]	22.5 ± 4.2	6.8 ± 0.2

[a] Surface-averaged, calculated as $\Sigma n_i d_i^3/\Sigma n_i d_i^2$, in which d_i is the particle diameter, [b] Calculated based on Au surface atoms obtained from surface-averaged particle size, considering that the fraction of Au surface atoms corresponds to the overall Au fraction, [c] A is the pre-exponential factor, [d] Based on Ag content.

The Ag catalyst starts to hydrogenate butadiene at 120 °C and barely reaches 15% conversion of butadiene at 300 °C. At 120 °C, the Ag catalyst is an order of magnitude less active than the Au catalyst. The Ag catalysts are reported to have comparable or even higher activity than Au catalysts in liquid-phase hydrogenation,[16,18,33] however, for gas-phase hydrogenation of *m*-dinitrobenzene, a carbon-supported Ag catalyst is reported to be five times less active than a similar Au catalyst.[34] The activation energy for the gas-phase hydrogenation of butadiene is 22.5 $kJ\,mol^{-1}$ for the Ag catalyst (Table 2 and Figure S.4). It is slightly different from the reported value of 38.4 $kJ\,mol^{-1}$ (for this reaction but performed in different conditions and determined in the temperature range of 50–110 °C),[13b] but less than half of that for the Au catalyst. This is in line with reports showing that Ag catalysts are in principle more active than Au in H_2 dissociation,[20] which is often the rate limiting step in hydrogenation reactions for Au.[31] The lower activity of Ag catalyst, despite its low activation energy, can be ascribed to the pre-exponential factor in the Arrhenius model, which is three orders of magnitude lower than that for Au (Table 2). In other words, apparently it is the low probability

of the reactants to be adsorbed on relevant sites on the Ag nanoparticles surface which causes the low conversion in this gas-phase reaction, although this is less of a limiting factor for (low temperature) liquid-phase hydrogenation reactions. This might be caused by inherently small heat of adsorption of the butadiene on the Ag surface at these temperatures, or by competitive adsorption of intermediates, products or other species present in the reaction mixture. Ag is active for hydrogenation reactions that involved oxygen containing substrates such as crotonaldehyde[14] can support this hypothesis, as high affinity of Ag for oxygen might lead to a higher heat of adsorption of the substrates and therefore a higher activity.

The Au–Ag bimetallic catalysts show activities intermediate between that of Au and that of Ag (Figure 3). Notably, at 120 °C, the apparent activation energy (Table 2), deduced from the corresponding Arrhenius plots (Figure S.4), is very similar for all Au-containing catalysts. This strongly suggests, as might be expected given the much lower activity of Ag, that the reaction on the Au surface atoms dominates. Table 2 shows the TOF of the catalysts based on the assumptions that only Au surface atoms are active (because the activity of Ag was negligible), and that the fraction of Au atoms of the surface is the same as the overall Au fraction, assuming that an alloy had formed. It seems a valid assumption, as we in situ reduced all the catalysts at 450 °C, and Au–Ag alloy formation upon high temperature reduction has been already reported by Mou et al.[35] The TOF per Au surface atom is constant and independent of the metal nanoparticle composition: there is apparently no significant influence owing to nearby Ag atoms on the activity of the individual Au surface atoms. Synergistic effect for Au–Ag catalysts have been previously reported mainly for oxidation reactions.[22a,b,36] For instance, Zheng et al. reported synergistic effects for Au–Ag catalysts with atomic Au to Ag ratios of 4 in the dehydrogenation of benzyl alcohol.[36b] For the selective hydrogenation of acetylene, Liu et al. reported slightly higher activities for the Au–Ag catalysts than for the Au catalysts. The catalysts were prepared by the same method that is used in the present study, but they obtained larger Au nanoparticles (4.9 nm). The higher activity of Au–Ag catalyst might be attributed to its smaller particle size (2.9 nm) rather than to Au–Ag synergism.[23b] For liquid-phase hydrogenation reaction, Qiang Xu et al. reported a synergistic effect for Au–Ag core–shell structure for reduction of *p*-nitrophenol[37] and showed that the synergistic effect is getting weaker if the Au and Ag formed alloy. However, Yang et al reported the synergistic effect for alloyed Au–Ag catalysts for the hydrogenation of crotonaldehyde.[38] Thus, it appears that for gas-phase butadiene hydrogenation reaction there is no evidence of a synergistic effect for Au–Ag catalysts.

Selectivity

Figure S.5 shows the evolution of the concentrations of all the reactants and products for the catalysts in the temperature range of 50–300 °C. The main products of the hydrogenation of butadiene in decreasing concentration are 1-butene, *cis*-2-butene, and *trans*-2-butene. This is consistent with the reported selectivities for Au catalysts for the hydrogenation of butadiene.[31,39] The butane concentration is below the detection limit for all the catalysts. To compare the selectivity of the Au catalyst to that of the bimetallic Au–Ag catalysts, the propene conversions versus butadiene conversion were extracted from the Figure S.5 and are plotted in Figure 4. For the Au catalyst at full conversion of butadiene, the propene conversion is only 0.1 % indicating that the Au catalyst is very selective towards hydrogenation of butadiene.

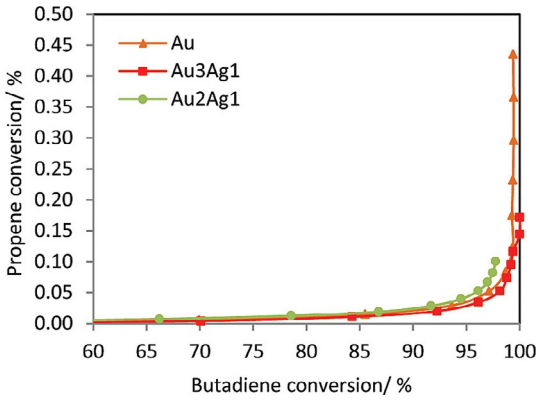

Figure 4. Propene conversions at different butadiene conversions for Au, Au2Ag1, and Au3Ag1 catalysts. Reaction mixture: 0.3 % butadiene, 30 % propene, 20 % H_2, and He for balance, flow rate 50 mL min^{-1}.

As the activity of the Ag catalyst is low, measuring the selectivity accurately is difficult (Figure S.5 d). Concerning the bimetallic catalysts, for the Au3Ag1 catalyst at full conversion of butadiene, propene conversion is also close to 0.1 %. Hence the bimetallic Au–Ag catalysts display high selectivities at 100 % butadiene conversion similar to the Au catalyst, and the presence of Ag has no influence on the selectivity of the Au atoms at the surface.

Stability

The catalyst stability was assessed by monitoring the butadiene conversion at 200 °C over 21 hours (Figure 5). The Au catalyst shows 96 % initial conversion and no significant decrease in conversion over 21 hours. We previously reported the high stability of Au supported on silica for the selective hydrogenation of butadiene.[40] In contrast, the Au–Ag catalysts gradually loose activity. The Au3Ag1 catalyst initially converts 77 % of the butadiene, and only 47 % after 21 hours on stream. The main activity loss occurs within the first 5 hours. The Au2Ag1 catalyst shows a very similar profile.

Deactivation by deposition of carbonaceous species is a first possibility and the main cause of deactivation for Pd catalysts used for the selective hydrogenation of butadiene in industry.[5,41] Figure 6 compares the weight loss monitored during TGA for the Au and Au3Ag1 catalysts, before and after 20 hours of catalysis. Although some carbonaceous species are formed during reaction, the amounts deposited for both catalysts seem very similar and hence the deposition of

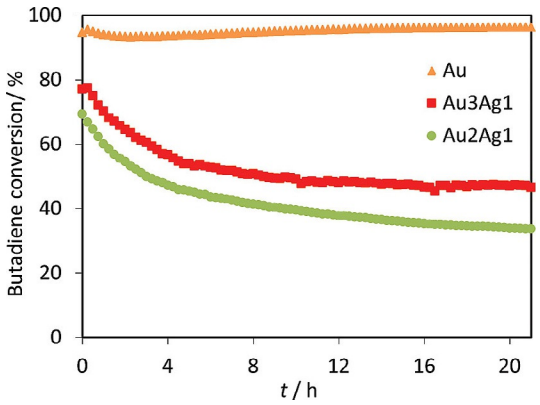

Figure 5. Evolution of the butadiene conversion for the Au (45 mg) and Au–Ag catalysts: Au3Ag1 (68 mg) and Au2Ag1 (75 mg) at 200 °C. Reaction mixture: 0.3 % butadiene, 30 % propene, 20 % H_2, and He for balance, flow rate 50 mL min^{-1}.

carbonaceous species can likely not explain the difference in stability. A second common reason for catalyst deactivation is metal particle growth. Crystallite sizes of the Au3Ag1 catalyst before and after catalysis are the same (3.8 and 3.9 nm, respectively). Furthermore, the initial activity of the Au–Ag catalysts was regenerated by in situ oxidation and reduction of the spent catalyst (at 450 °C, Figure S.6). As metal particle growth is in general not reversible, it cannot be considered as the reason for the loss of activity.

Specifically for bimetallic catalysts, an additional reason for deactivation can be the rearrangement of the metal atoms within the nanoparticles. Notably, the time scale of this rearrangement for particles of 3–4 nm at 200 °C, using Fick's first law of diffusion and the bulk diffusion coefficient of Au metal of 10^{-22} m^2 s^{-1},[42] corresponds to the deactivation time scale which is around 5 h for both Au–Ag catalysts. The surface composition of the Au–Ag catalysts was assessed using near ambient pressure (NAP) XPS under vacuum and H_2 atmosphere at photon energies of 500 and 700 eV. This experiment could not be performed in the presence of butadiene because hydrocarbons decompose in the beam, resulting in carbon contamination. The inelastic mean free path of both Au and Ag is short (0.7 nm at 500 eV[43] and 1.0 nm at 700 eV). Hence, especially at 500 eV the measurements preferentially probe the surface, despite an Au–Ag particle size of only 3.4 nm.

Photo-emission spectra of the Au2Ag1 catalyst at photon energies of 700 and 500 eV are shown in Figure S.7. Quantification of the areas of the Au 4 f and the Ag 3 d peaks is given in Table 3 (more detailed information in Table S.1). The higher Ag/Au ratio at photon energy of 500 eV than the one at 700 eV suggests that at room temperature and under vacuum, Ag preferentially resides already near the surface. This might be explained by the lower tabulated vacuum surface energy of Ag in comparison to Au.[44] Subsequently, the samples were exposed to 100 Pa of H_2 and gradually heated. The spectra show (Figure S.7 and Table 3) no effect of the H_2 exposure at room temperature or 135 °C, but upon heating to 210 °C the fraction of Ag atoms near the particle surface increases. As these measurements are very time consuming, it was not possible to run similar heating experiments under UHV to see if the Ag surface enrichment also occurs in vacuum. However, Au and Ag are miscible at all temperatures, and at higher temperature, entropy effect normally leads to alloy formation rather than the phase segregation, it can safely be assumed that Ag surface enrichment is a result of H_2 exposure and not just owing to heating.

Table 3. Quantification on the Au 4 f and Ag 3 d peaks obtained from the photo-emission spectra of the Au2Ag1 catalyst.

Photon energy (eV)	Condition	T [°C]	Ag/Au ratio
700	UHV	RT	1.5
500	UHV	RT	2.4
500	100 Pa	RT	2.2
500	100 Pa	135	2.4
500	100 Pa	210	3.4

It is known from literature,[35,45] that heating in an oxidizing atmosphere leads to Ag surface enrichment, and high temperature reduction reverses it to form an Au–Ag alloy. However, this is the first time that it is shown that at intermediate temperatures H_2 exposure induces Ag atoms segregation to the surface of Au–Ag nanoparticles. The driving force for such

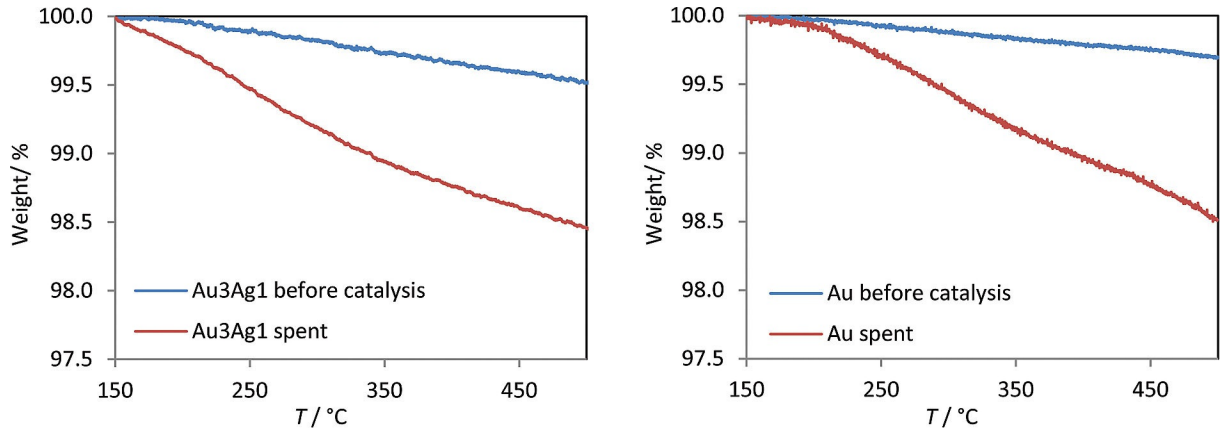

Figure 6. Mass loss of the Au3Ag1 (left) and Au (right) samples during heating with 5 °C min^{-1} under a 10 mL min^{-1} flow of oxygen.

segregation can be a stronger Ag–H bonding than the Au–H bonding suggested by Hammer et al.[20] Notably, in the NAP-XPS experiments, H_2 pressure is only 100 Pa which is far less than the 20 kPa partial pressure of H_2 under reaction conditions, under which the driving force for Ag segregation is probably much higher. Hence one can assume that under reaction conditions at 200 °C a gradual enrichment of the surface of these bimetallic particles by Ag also occurs. As Ag is less active for the hydrogenation of butadiene than Au, this atomic redistribution can explain why the bimetallic catalysts gradually deactivate whereas the monometallic Au catalyst remains stable. The catalytic activity of the Au–Ag catalysts is revived by high temperature oxidation/reduction (Figure S.6) and is related to reformation of the Au–Ag alloy, and hence confirms the rearrangement of the metal atoms within the nanoparticles as a major cause of bimetallic catalyst deactivation.

Conclusions

The activity, selectivity, and stability of the Au, Ag, and Au–Ag catalysts, as model bimetallic catalysts, for the gas-phase selective hydrogenation of butadiene in a propene gas stream were investigated. The Au catalyst was more than an order of magnitude more active than the Ag catalyst at 120 °C. The low activity of the Ag catalysts, despite lower activation energy for the reaction than for Au, was ascribed to the low concentration of butadiene molecules adsorbed on the Ag surface under these conditions. All Au-containing catalysts were selective, and equally active if the activity is normalized per Au content; hence the presence of Ag does not affect either initial activity or selectivity of the Au in the bimetallic particles. These results highlight the sometimes very different behavior of catalysts in liquid and gas-phase oxidation reactions. Although the Au catalyst was stable, the bimetallic catalysts showed a gradual activity loss during the first 5 h on stream at 200 °C, which was explained by the segregation of the less active Ag atoms to the surface under reaction conditions. The initial activity of the bimetallic catalysts was restored after regeneration by oxidation/reduction at 450 °C. Furthermore, it is the first report of Ag surface segregation under H_2, illustrating the sensitivity of bimetallic Au–Ag catalysts to atomic rearrangement under reaction conditions.

Experimental Section

Catalyst preparation

The silica support (SBA-15, 1 g, BET surface area 800 $m^2 g^{-1}$) was prepared by the method of Sayari et al.[29] In a typical preparation, poly (ethylene oxide)-*block*-poly (propylene oxide)-*block*-poly (ethylene oxide) triblock copolymer (4.0 g, $EO_{20}PO_{70}EO_{20}$, Pluronic P123, M_{av} = 5800, Sigma Aldrich) was dissolved in mixture of aqueous HCl (120 g, 2 M) and water (30 g) at room temperature. After at least 45 min at 35 °C, tetraethoxysilane (8.5 g) was added and the solution was stirred for 5 min. After 20 h at 38 °C under static conditions, the cloudy mixture was kept at 90 °C for 24 h. The precipitate was filtered and washed at room temperature (RT) until all chloride ions were removed and subsequently dried at 60 °C in static air overnight. Then the precipitate was calcined at 550 °C in static air for 6 h to yield SBA-15.

The silica support was functionalized using aminopropyl triethoxysilane (APTES).[46] First, the support was dried at 140 °C under vacuum for 24 h. Then, dry toluene (50 mL) and APTES (1 g) were added. The amount of APTES needed for covering the support surface was calculated based on the BET surface area of the SBA-15, considering three OH groups per nm^2 for silica.[47] The mixture was refluxed for 24 h at 110 °C in an N_2 atmosphere. The functionalized silica was recovered by centrifugation, washed with ethanol (40 mL) twice at RT, and dried at 60 °C in static air overnight.

The metals were deposited following the method of Mou et al.[35a] The functionalized silica (1 g) was dispersed in water (15 mL, doubled distilled). To prepare the monometallic Au or Ag catalyst, either a $HAuCl_4.3H_2O$ aqueous solution (0.05 M, 3 mL) or an $AgNO_3$ aqueous solution (0.05 M, 3 mL) was added, and the mixture was stirred at RT for 2 h. The powder was recovered by centrifugation and washed twice with water at RT. Then, the powder was redispersed in water (15 mL), and the metal ions reduced by a rapid addition of $NaBH_4$ solution (0.2 M, 5 mL) under vigorous stirring at RT. After 20 min, the product was collected by centrifugation, washed with water (80 mL) twice at RT and dried at 60 °C in static air overnight.

Following this, to prepare Au–Ag catalysts, Ag was deposited on the Au/SBA15 keeping the total mole percentage of metal constant to ensure an atomic ratio (Au:Ag) of 3:1 and 2:1, which are denoted as Au3Ag1 and Au2Ag1, respectively. To eliminate the amine groups, the catalysts were calcined either at 500 °C for Au and Au–Ag catalysts, or at 450 °C for the Ag catalyst in static air for 4 h. The Ag catalyst was calcined at lower temperatures to limit particle growth.

Characterization

To obtain suitable samples for transmission electron microscopy (TEM) characterization, the samples were cut into slices of 70 nm thickness using an Ultracut E Reichert-Jung microtome (Leica). TEM imaging was performed on a Tecnai 12 (FEI) microscope operated at 120 kV. To assure Ag nanoparticles are imaged properly, high angle annular dark-field scanning transmission electron microscopy was performed on a Tecnai 20 (FEG) microscope operated at 200 kV. Particle sizes were determined from the TEM images by measuring the sizes of typically 300 individual particles on different areas of the sample. XRD was performed with a Bruker D2 phaser with $Co_{K\alpha}$ source. Elemental analysis was performed using inductively coupled plasma-mass spectrometry at the Mikroanalytisches Laboratorium Kolbe, Germany. UV/Vis analysis was performed on a VARIAN 5000 spectrometer. Nitrogen physisorption measurements were done at −196 °C (77 K) (Micromeritics, TriStar 3000). Thermogravimetric analysis (TGA) was performed on a PerkinElmer (Pris 1) connected to a mass detector. The powder sample (approximately 10 mg) heated for 30 min at 150 °C and further heated to 800 °C (5 °C min^{-1}) under a flow of oxygen (10 mL min^{-1}) over the sample.

Catalytic tests

The hydrogenation of butadiene was performed at atmospheric pressure in a pyrex plug flow reactor (internal diameter 4 mm). To test the activity and the selectivity, 100 mg catalyst (sieve fraction,

150–212 μm) was exposed to a reaction mixture which consisted of 0.3% butadiene, 30% propene, 20% H_2, and helium as balance with a flow rate of 50 mL min^{-1} (normal temperature and pressure conditions, gas hourly space velocity (GHSV) = 11 700 h^{-1}). The catalyst was heated at a rate of 1 °C min^{-1}, from RT to 300 °C, while monitoring the product flow every 15 min with online gas chromatography (Perichrom PR 2100, column filled with sebaconitrile 25% Chromosorb PAW 80/100 Mesh, FID (flame ionization detector).

To verify that the reaction was not mass transfer limited, Au catalysts with different sieve fractions (75–150, 150–212 and 212–425 μm) were tested. Half the amount of catalyst with the same GHSV was tested as well. The activity was similar in all these tests within the range of 6% of conversion of butadiene at 120 °C, showing that there were no internal or external mass transfer limitations.

After cooling down to RT, the same catalyst was reduced in situ under pure H_2 (100 mL min^{-1}) from RT to 450 °C (ramp 2 °C min^{-1}) and kept at 450 °C for 180 min to test the effect of reduction on the activity. The activity and selectivity of the same catalyst was subsequently tested again.

Turnover frequencies (TOF) were calculated from the activity × M_{Au}/D, in which M_{Au} is Au molecular weight, and D is $6(v_m/a_m)/d_{VA}$. Here, a_m is the area occupied by a surface atom, v_m is volume occupied by an atom in bulk metal, and d_{VA} is the surface-averaged particle size.[48] The apparent activation energy was calculated from the Arrhenius plots (ln (activity) versus 1/T) in the range of 75–120 °C, as in this temperature range the reaction is zero order with respect to butadiene.[31] The pre-exponential factor was calculated from the intercept.

For the stability tests, either Au catalyst (45 mg) or Au3Ag1 (68 mg) catalyst or Au2Ag1 (75 mg) catalyst, which contain the same amount of Au in mole, were loaded into the reactor. After in situ reduction, the reactor was cooled and maintained at 200 °C, and the catalytic reaction was performed for 21 h.

Regeneration was performed after a stability test on Au2Ag1 catalyst in situ by consecutive oxidation (air flow, 100 mL min^{-1}) and reduction (H_2 flow, 100 mL min^{-1}) both for 180 min at 450 °C followed by another stability test.

NAP-XPS experiment

The near ambient pressure (NAP) XPS experiments were performed on branch 2 of the TEMPO beamline of the SOLEIL synchrotron radiation facility in Paris,[49] using the NAP-XPS end station of Paris 6 University. It is equipped with a SPECS Phoibos 150-NAP electron analyzer, the detector is a 3D(*x*, *y*, t) delay detector. The base pressure in the main chamber is in the low 10^{-7} Pa and XPS can in principle be performed up to 2.5 KPa, the photon beam enters the chamber through a windowless aperture differentially pumped. At a photon energy of 500 eV and a pass energy of 50 eV, the overall resolution is greater than 0.2 eV. The emitted electrons are collected at normal emergence from the sample and the probe size was 100 × 100 μm^2. The experiments were performed on the Au2Ag1 catalyst. To compensate charge effects, carbon nanotubes (1 wt.%) were dispersed in the sample by sonication in ethanol. After the sample was dried, a copper grid (used for TEM) with window size 200 × 200 μm^2 was pressed on a thin layer of powder samples to limit the surface charging. The grid was mounted on a handmade XPS sample holder (Figure S.8).

The sample position was optimized by minimizing the copper intensity. To obtain the surface composition, the photo-emission spectra were collected under ultra-high vacuum (10^{-7} Pa) with photon energy of 500 eV and 700 eV at RT. Au and Ag XPS regions were obtained by adding up 40 individual spectrum, and Si and C XPS regions were obtained from a single spectrum (step size of 0.1 eV and step time of 0.1 s). To investigate the effect of H_2 on the surface composition, the analyzer chamber was pressurized with 100 Pa of H_2. The sample was heated using a button heater (filament in Al_2O_3 ceramic) and the temperature measured with a K-type thermocouple. The temperature was controlled by increasing manually but gradually the heater output to have a heating rate of around 5 °C min^{-1}. The series of spectra were collected at around 135 and 210 °C ± 10 °C (dwell time of 30 min at each step before collecting spectra) with photon energy of 500 eV. Background correction was performed by using a Shirley background and the spectra were calibrated with respect to the Si2p peak. The spectra were fitted using Casa XPS v.2.3.16 software (Casa Software Ldt, UK) with voigt profile applying a Gaussian/Lorentzian ratio equal to 70/30. For semi-quantitative analysis, the Au:Ag ratio was calculated from the measured Au 4 $f_{5/2}$ and Ag 3 $d_{3/2}$ intensities weighted by their respective photoionization cross section.

Acknowledgements

We gratefully acknowledge Hans Meeldijk for TEM imaging, Marjan Versluijs-Helder for TGA, Marcel van Asselen for designing and building the XPS sample holder, and the scientific staff of the TEMPO beamline, Soleil synchrotron radiation facility in Paris: Dr Ahmed Naitabdi, Anthony Boucly, and Georgia Olivieri. We are grateful to Utrecht University for a short stay PhD fellowship and NWO-Vici (16.130.344) for overall funding of the project.

Conflict of interest

The authors declare no conflict of interest.

Keywords: atomic rearrangements · Au–Ag · heterogeneous catalysis · hydrogenation · photoelectron spectroscopy

[1] J. Saavedra, H. A. Doan, C. J. Pursell, L. C. Grabow, B. D. Chandler, *Science* **2014**, *345*, 1599 – 1602.
[2] a) R. Zanella, C. Louis, S. Giorgio, R. Touroude, *J. Catal.* **2004**, *223*, 328 – 339; b) T. Mitsudome, K. Kaneda, *Green Chem.* **2013**, *15*, 2636.
[3] T. Takei, T. Akita, I. Nakamura, T. Fujitani, M. Okumura, K. Okazaki, J. Huang, T. Ishida, M. Haruta, *Adv. Catal.* **2012**, *55*, 1 – 126.
[4] X. L. Yan, J. Wheeler, B. Jang, W. Y. Lin, B. R. Zhao, *Appl. Catal. A* **2014**, *487*, 36 – 44.
[5] A. Hugon, L. Delannoy, C. Louis, *Gold Bull.* **2008**, *41*, 127 – 138.
[6] a) A. P. Umpierre, G. Machado, G. H. Fecher, J. Morais, J. Dupont, *Adv. Synth. Catal.* **2005**, *347*, 1404 – 1412; b) M. Bender, *ChemBioEng. Rev.* **2014**, *1*, 136 – 147.
[7] a) M. L. Derrien, in *Catalytic hydrogenation, Vol. 27* (Ed.: L. Cerveny), Elsevier, **1986**, p. 613; b) M. Baerns in *Springer Series in Chemical Physics, Vol. 75*, (Eds.: A. W. Castleman, J. P. Toennies, K. Yamanouchi, W. Zinth), Springer, **2004**, pp. 117 – 119; c) http://www.jmprotech.com/olefins-catalysts-johnson-matthey.
[8] N. E. Kolli, L. Delannoy, C. Louis, *J. Catal.* **2013**, *297*, 79 – 92.
[9] P. Wells, *J. Catal.* **1978**, *52*, 498 – 506.
[10] a) F. Cárdenas-Lizana, S. Gómez-Quero, C. J. Baddeley, M. A. Keane, *Appl. Catal. A* **2010**, *387*, 155 – 165; b) A. Aguilar-Tapia, L. Delannoy, C. Louis, C. W. Han, V. Ortalan, R. Zanella, *J. Catal.* **2016**, *344*, 515 – 523.

[11] A. Hugon, L. Delannoy, J. M. Krafft, C. Louis, *J. Phys. Chem. C* **2010**, *114*, 10823 – 10835.
[12] L. Delannoy, G. Thrimurthulu, P. S. Reddy, C. Methivier, J. Nelayah, B. M. Reddy, C. Ricolleau, C. Louis, *Phys. Chem. Chem. Phys.* **2014**, *16*, 26514 – 26527.
[13] a) J. Hohmeyer, E. V. Kondratenko, M. Bron, J. Krohnert, F. C. Jentoft, R. Schlögl, P. Claus, *J. Catal.* **2010**, *269*, 5 – 14; b) A. Sárkány, Z. Révay, *Appl. Catal. A* **2003**, *243*, 347 – 355.
[14] a) H. J. Wei, C. Gomez, J. J. Liu, N. Guo, T. P. Wu, R. Lobo-Lapidus, C. L. Marshall, J. T. Miller, R. J. Meyer, *J. Catal.* **2013**, *298*, 18 – 26; b) M. Bron, D. Teschner, A. Knop-Gericke, F. C. Jentoft, J. Krohnert, J. Hohmeyer, C. Volckmar, B. Steinhauer, R. Schlogl, P. Claus, *Phys. Chem. Chem. Phys.* **2007**, *9*, 3559 – 3569; c) X. F. Yang, A. Q. Wang, X. D. Wang, T. Zhang, K. L. Han, J. Li, *J. Phys. Chem. C* **2009**, *113*, 20918 – 20926.
[15] M. Steffan, A. Jakob, P. Claus, H. Lang, *Catal. Commun.* **2009**, *10*, 437 – 441.
[16] J. W. Zheng, H. Q. Lin, Y. N. Wang, X. L. Zheng, X. P. Duan, Y. Z. Yuan, *J. Catal.* **2013**, *297*, 110 – 118.
[17] K. Shimizu, Y. Miyamoto, A. Satsuma, *J. Catal.* **2010**, *270*, 86 – 94.
[18] G. Vilé, J. Perez-Ramirez, *Nanoscale* **2014**, *6*, 13476 – 13482.
[19] W. Grünert, A. Bruckner, H. Hofmeister, P. Claus, *J. Phys. Chem. B* **2004**, *108*, 5709 – 5717.
[20] B. Hammer, J. K. Norskov, *Nature* **1995**, *376*, 238 – 240.
[21] a) B. Bridier, N. Lopez, J. Perez-Ramirez, *Dalton Trans.* **2010**, *39*, 8412 – 8419; b) F. R. Lucci, J. Liu, M. D. Marcinkowski, M. Yang, L. F. Allard, M. Flytzani-Stephanopoulos, E. C. Sykes, *Nat. Commun.* **2015**, *6*, 8550.
[22] a) A. Sandoval, A. Aguilar, C. Louis, A. Traverse, R. Zanella, *J. Catal.* **2011**, *281*, 40 – 49; b) T. Benkó, A. Beck, K. Frey, D. F. Sranko, O. Geszti, G. Safran, B. Maroti, Z. Schay, *Appl. Catal. A* **2014**, *479*, 103 – 111; c) G. Nagy, T. Benkó, L. Borkó, T. Csay, A. Horváth, K. Frey, A. Beck, *React. Kinet. Mech. Catal.* **2015**, *115*, 45 – 65; d) A. Sandoval, L. Delannoy, C. Méthivier, C. Louis, R. Zanella, *Appl. Catal. A* **2015**, *504*, 287 – 294.
[23] a) A. Q. Wang, X. Y. Liu, C. Y. Mou, T. Zhang, *J. Catal.* **2013**, *308*, 258 – 271; b) X. Liu, Y. Li, J. W. Lee, C.-Y. Hong, C.-Y. Mou, B. W. L. Jang, *Appl. Catal. A* **2012**, *439 – 440*, 8 – 14.
[24] a) M. J. Walsh, K. Yoshida, M. L. Pay, P. L. Gai, E. D. Boyes, *ChemCatChem* **2012**, *4*, 1638 – 1644; b) C. Louis, C. Bond, *Catalysis by gold*, Imperial College Press, **2006**.
[25] a) Y. Chen, Q. Wang, T. Wang, *Dalton Trans.* **2013**, *42*, 13940 – 13947; b) W. Yu, M. D. Porosoff, J. G. Chen, *Chem. Rev.* **2012**, *112*, 5780 – 5817.
[26] A. Sandoval, C. Louis, R. Zanella, *Appl. Catal. B* **2013**, *140*, 363 – 377.
[27] V. Papaefthimiou, F. Tournus, A. Hillion, G. Khadra, D. Teschner, A. Knop-Gericke, V. Dupuis, S. Zafeiratos, *Chem. Mater.* **2014**, *26*, 1553 – 1560.
[28] a) Y. Z. Xiang, R. Barbosa, N. Kruse, *ACS Catal.* **2014**, *4*, 2792 – 2800; b) S. K. Beaumont, S. Alayoglu, V. V. Pushkarev, Z. Liu, N. Kruse, G. A. Somorjai, *Faraday Discuss.* **2013**, *162*, 31.
[29] A. Sayari, B. H. Han, Y. Yang, *J. Am. Chem. Soc.* **2004**, *126*, 14348 – 14349.
[30] a) M. B. Cortie, A. M. McDonagh, *Chem. Rev.* **2011**, *111*, 3713 – 3735; b) M. P. Mallin, C. J. Murphy, *Nano Lett.* **2002**, *2*, 1235 – 1237; c) W. Albrecht, J. E. van der Hoeven, T. S. Deng, P. E. de Jongh, A. van Blaaderen, *Nanoscale* **2017**, *9*, 2845 – 2851.
[31] A. Hugon, L. Delannoy, C. Louis, *Gold Bull.* **2009**, *42*, 310 – 320.
[32] a) M. Okumura, T. Akita, M. Haruta, *Catal. Today* **2002**, *74*, 265 – 269; b) X. Zhang, H. Shi, B. Q. Xu, *Angew. Chem. Int. Ed.* **2005**, *44*, 7132 – 7135; *Angew. Chem.* **2005**, *117*, 7294 – 7297.
[33] M. G. Prakash, R. Mahalakshmy, K. R. Krishnamurthy, B. Viswanathan, *Catal. Today* **2016**, *263*, 105 – 111.
[34] F. Cárdenas-Lizana, Z. M. De Pedro, S. Gomez-Quero, L. Kiwi-Minsker, M. A. Keane, *J. Mol. Catal. A* **2015**, *408*, 138 – 146.
[35] a) X. Y. Liu, A. Q. Wang, X. F. Yang, T. Zhang, C. Y. Mou, D. S. Su, J. Li, *Chem. Mater.* **2009**, *21*, 410 – 418; b) A. Q. Wang, C. M. Chang, C. Y. Mou, *J. Phys. Chem. B* **2005**, *109*, 18860 – 18867.
[36] a) J. H. Liu, A. Q. Wang, Y. S. Chi, H. P. Lin, C. Y. Mou, *J. Phys. Chem. B* **2005**, *109*, 40 – 43; b) J. Zheng, J. Qu, H. Lin, Q. Zhang, X. Yuan, Y. Yang, Y. Yuan, *ACS Catal.* **2016**, *6*, 6662 – 6669.
[37] H. L. Jiang, T. Akita, T. Ishida, M. Haruta, Q. Xu, *J. Am. Chem. Soc.* **2011**, *133*, 1304 – 1306.
[38] H. Q. Lin, J. W. Zheng, X. L. Zheng, Z. Q. Gu, Y. Z. Yuan, Y. H. Yang, *J. Catal.* **2015**, *330*, 135 – 144.
[39] X.-F. Yang, A.-Q. Wang, Y.-L. Wang, T. Zhang, J. Li, *J. Phys. Chem. C* **2010**, *114*, 3131 – 3139.
[40] N. Masoud, L. Delannoy, H. Schaink, A. v. d. Eerden, J. d. Rijk, T. A. G. Silva, D. Banerjee, J. D. Meeldijk, K. P. de Jong, C. Louis, P. E. de Jongh, *unpublished results*.
[41] B. K. Furlong, J. W. Hightower, T. Y. L. Chan, A. Sarkany, L. Guczi, *Appl. Catal. A* **1994**, *117*, 41 – 51.
[42] K. Dick, T. Dhanasekaran, Z. Zhang, D. Meisel, *J. Am. Chem. Soc.* **2002**, *124*, 2312 – 2317.
[43] C. J. Powell, A. Jablonski, *J. Phys. Chem. Ref. Data* **1999**, *28*, 19 – 62.
[44] A. L. Gould, C. J. Heard, A. J. Logsdail, C. R. A. Catlow, *Phys. Chem. Chem. Phys.* **2014**, *16*, 21049 – 21061.
[45] a) C.-W. Yen, M.-L. Lin, A. Wang, S.-A. Chen, J.-M. Chen, C.-Y. Mou, *J. Phys. Chem. C* **2009**, *113*, 17831 – 17839; b) S. Pramanik, S. Chattopadhyay, J. K. Das, U. Manju, G. De, *J. Mater. Chem. C* **2016**, *4*, 3571 – 3580.
[46] S. Shylesh, A. R. Singh, *J. Catal.* **2006**, *244*, 52 – 64.
[47] R. Mueller, H. K. Kammler, K. Wegner, S. E. Pratsinis, *Langmuir* **2003**, *19*, 160 – 165.
[48] K. S. W. Sing, J. Rouquer, *Handbook of Heterogeneous Catalysis*, VCH Verlagsgesellschaft mbH, **1997**.
[49] http://www.synchrotron-soleil.fr/recherche/lignelumiere/tempo.

Manuscript received: January 17, 2017
Revised manuscript received: May 3, 2017
Version of record online: June 12, 2017